

# Structure–Activity Relationship Studies and *Plasmodium* Life Cycle Profiling Identifies Pan-Active *N*-Aryl-3-trifluoromethyl Pyrido[1,2-*a*]benzimidazoles Which Are Efficacious in an *in Vivo* Mouse Model of Malaria

Godfrey Mayoka,<sup>†</sup> Mathew Njoroge,<sup>#</sup> John Okombo,<sup>†</sup> Liezl Gibhard,<sup>#</sup> Margarida Sanches-Vaz,<sup>‡</sup> Diana Fontinha,<sup>‡</sup> Lyn-Marie Birkholtz,<sup>∞</sup> Janette Reader,<sup>∞</sup> Mariëtte van der Watt,<sup>∞</sup> Theresa L. Coetzer,<sup>∇</sup> Sonja Lauterbach,<sup>∇</sup> Alisje Churchyard,<sup>∇</sup> Belinda Bezuidenhout,<sup>∇</sup> Timothy J. Egan,<sup>†,△,ID</sup> Clive Yeates,<sup>||</sup> Sergio Wittlin,<sup>Ψ,‡</sup> Miguel Prudêncio,<sup>‡</sup> and Kelly Chibale<sup>\*,†,§,△,ID</sup>

<sup>†</sup>Department of Chemistry, University of Cape Town, Rondebosch 7701, South Africa

<sup>#</sup>Drug Discovery and Development Centre (H3D), Division of Clinical Pharmacology, Department of Medicine, University of Cape Town, Observatory, Cape Town 7925, South Africa

<sup>∞</sup>Department of Biochemistry, Genetics and Microbiology, Institute for Sustainable Malaria Control, University of Pretoria, Private Bag X20, Hatfield 0028, South Africa

<sup>∇</sup>Wits Research Institute for Malaria, Faculty of Health Sciences, University of the Witwatersrand and National Health Laboratory Service, Johannesburg 2193, South Africa

<sup>||</sup>Inpharma Consultancy, 6 Dudley Hill Close, Welwyn, Hertfordshire AL60QQ, U.K.

<sup>‡</sup>Instituto de Medicina Molecular João Lobo Antunes, Faculdade de Medicina, Universidade de Lisboa, Av. Prof. Egas Moniz, 1649-028 Lisbon, Portugal

<sup>Ψ</sup>Department of Medical Parasitology and Infection Biology, Swiss Tropical and Public Health Institute, Basel, Switzerland

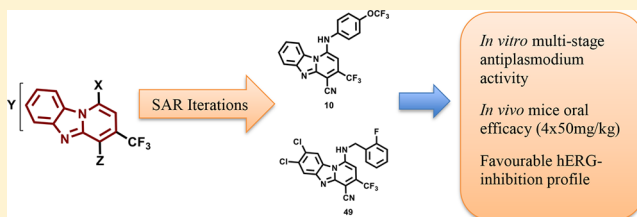
<sup>‡</sup>University of Basel, Basel, Switzerland

<sup>§</sup>South African Medical Research Council, Drug Discovery and Development Research Unit, University of Cape Town, Rondebosch 7701, South Africa

<sup>△</sup>Institute of Infectious Disease and Molecular Medicine, University of Cape Town, Rondebosch 7701, South Africa

## **S** Supporting Information

**ABSTRACT:** Structure–activity relationship studies involving *N*-aryl-3-trifluoromethyl pyrido[1,2-*a*]benzimidazoles (PBI) identified several compounds possessing potent *in vitro* activities against the asexual blood, liver, and gametocyte stages of the *Plasmodium* parasite with no cross-resistance to chloroquine. Frontrunner lead compounds with good *in vitro* absorption, distribution, metabolism, and excretion (ADME) profiles were subjected to *in vivo* proof-of-concept studies in NMRI mice harboring the rodent *P. berghei* infection. This led to the identification of compounds **10** and **49**, effecting 98% and 99.93% reduction in parasitemia with mean survival days of 12 and 14, respectively, at an oral dose of 4 × 50 mg/kg. *In vivo* pharmacokinetics studies on **10** revealed slow absorption, low volume of distribution, and low clearance profiles. Furthermore, this series displayed a low propensity to inhibit the human ether-a-go-go-related gene (hERG) potassium ion channel whose inhibition is associated with cardiotoxicity.



## ■ INTRODUCTION

Drug resistance is a perennial threat to the control of malaria, a disease concentrated mainly in the tropical and subtropical regions of the world, with disproportionate endemicity in Africa.<sup>1</sup> Malaria is transmitted by parasites of the *Plasmodium* genus with five species known to infect humans: *P. falciparum*, *P. malariae*, *P. vivax*, *P. ovale*, and *P. knowlesi*, with infections by *P. falciparum* and *P. vivax* being the most virulent and widespread.<sup>2–5</sup> Human malaria infection is initiated when a

female anopheles mosquito deposits sporozoites during a blood meal. These sporozoites migrate to the liver where they undergo further development into schizonts which produce merozoites that enter the systemic circulation where they infect red blood cells and cause the typical symptoms of malaria.<sup>6</sup> A subset of the liver stage parasites, however, remain dormant in

Received: November 13, 2018

Published: December 18, 2018

a form known as hypnozoites in the case of malaria caused by *P. ovale* and *P. vivax* parasites. These hypnozoites can be reactivated in future to initiate blood stage infections.<sup>5</sup> On the other hand, some of the asexual blood stage parasites transform into male and female gametocytes which are taken up by a mosquito during a blood meal, fuse within the midgut of the mosquito to form a zygote which later differentiates into sporozoites. The sporozoites are introduced into humans during a mosquito bite, thus completing the life cycle of the parasite.<sup>7</sup>

The socio-economic and public health impact of malaria is startling: hundreds of thousands of lives are lost annually, in addition to major indirect losses in terms of productivity and human capacity development, as assessed by disability- and quality-adjusted life years (DALYS and QALYS, respectively). Thus, malaria seems to perpetuate cycles of poverty in countries where it is rife.<sup>8</sup> Chemotherapy remains a fundamental component of malaria control, in addition to public health approaches that focus on vector control and vaccine development.<sup>9–13</sup> Unfortunately, the decreased efficacy of even the most promising antimalarial agents in some regions threatens a reversal of gains in the malaria elimination agenda.<sup>14–16</sup> Furthermore, the treatment, control, and eradication of malaria hinges on targeting all the life cycle stages of *Plasmodium*; a profile that most standard antimalarial drugs lack. For example, primaquine is the only antimalarial drug with good activity against late stage gametocytes<sup>17</sup> and, together with tafenoquine, is effective in preventing relapse due to *Plasmodium vivax* malaria infections. Unfortunately, the two drugs are beset by toxicity concerns in patients with Glucose-6-phosphate dehydrogenase (G6PD) enzyme deficiency.<sup>18</sup> The above-described scenarios, therefore, warrant sustained efforts in the discovery and development of new antimalarial drugs as suitable alternatives to currently existing ones and having transmission-blocking potential.

The tricyclic pyridobenzimidazole (PBI) scaffold has emerged as an important medicinal chemistry substructure with several pharmacological and biological activities reported including antifungal, antibacterial, antiviral, and antitumor.<sup>19–21</sup> Our group has previously reported on the antimalarial properties of PBI derivatives following medicinal chemistry iterations based on phenotypic whole cell screening hits against the human parasite *P. falciparum*.<sup>22</sup> Although the mechanism of the antimalarial action of these compounds remain unresolved, targeting the hemoglobin degradation pathway has been proposed based on structural congruences the PBIs share with canonical inhibitors of this process such as the aminoquinoline antimalarials. In the present work, antiplasmodium structure–activity relationship (SAR) studies focusing on *N*-aryl substitutions on a 3-trifluoromethyl PBI nucleus were evaluated (Figure 1). In line with most drug discovery programs, analogues from this study were also profiled for their inhibition of the human ether-a-go-go-related gene (hERG)-encoded potassium ion channels to understand cardiotoxicity risks that may be associated with this series. Herein, we report the identification of potent, multistage active analogues with an attractive hERG potassium ion channel inhibition profile along with good *in vivo* efficacy in a murine model of malaria. The pharmacokinetics profile of a representative lead compound, **10**, following oral and intravenous administration in mice is also reported.

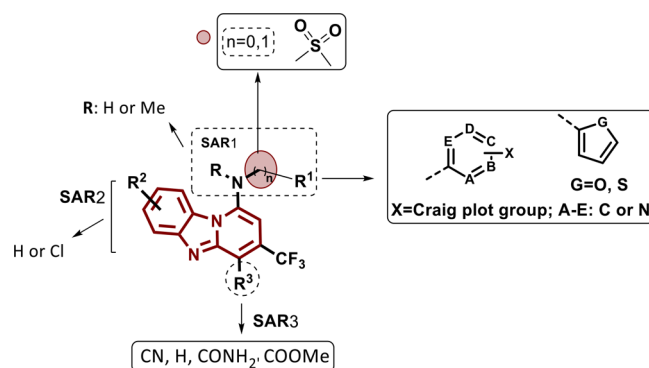


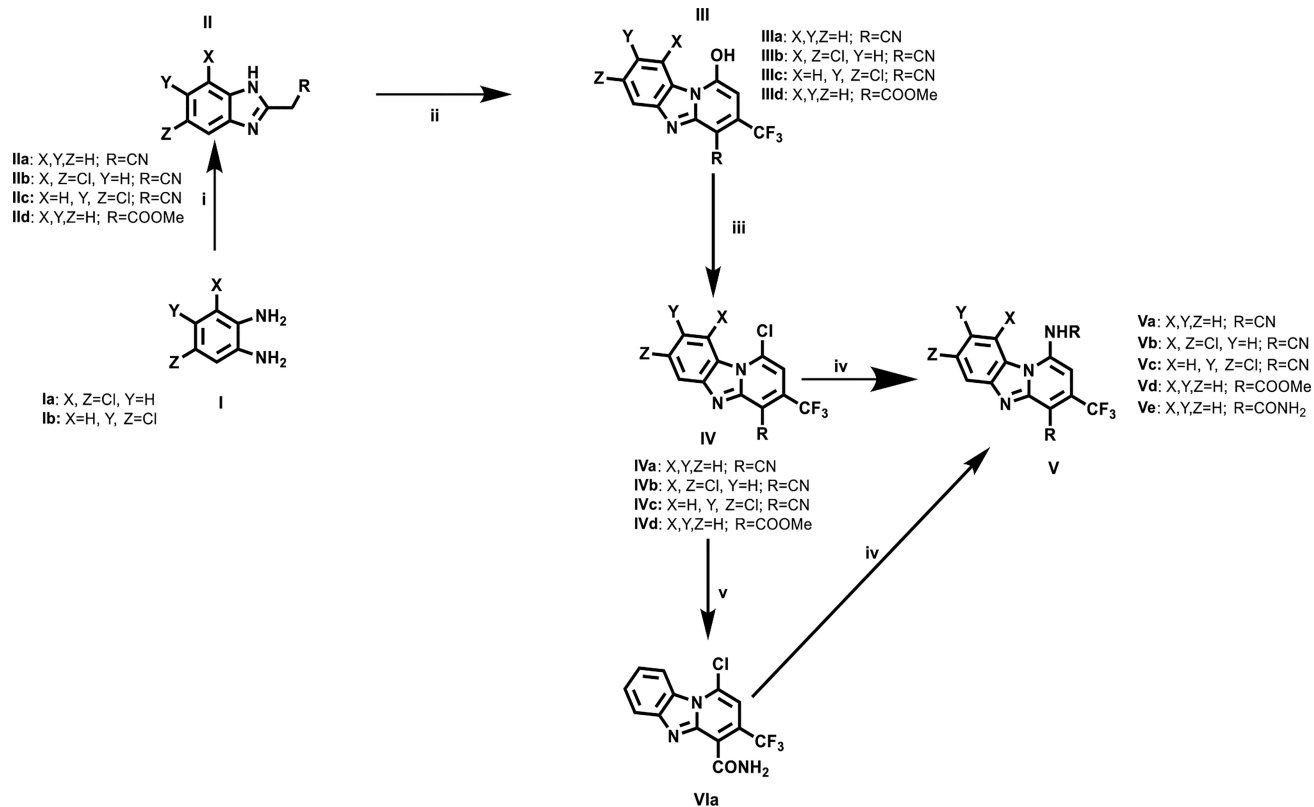
Figure 1. SAR strategy around the 3-trifluoromethyl PBI scaffold.

## RESULTS AND DISCUSSION

**Chemistry.** Target compounds were prepared as previously described (Scheme 1).<sup>23</sup> Briefly, compounds devoid of substitution on the left-hand side were synthesized from commercially sourced 2-benzimidazole acetonitrile (**IIa**). For other targets, the corresponding substituted diamino benzene starting material (**I**) was condensed with ethyl-2-cyanoacetate to form the equally substituted benzimidazole acetonitrile derivative (**IIb** and **IIc**). Subsequently, the benzimidazole acetonitrile and ethyl 4,4,4-trifluoro-3-oxobutanoate were condensed in the presence of ammonium acetate to provide the tricyclic hydroxyl intermediate (**III**), which is converted to the penultimate chloro intermediate (**IV**) using phosphoryl trichloride ( $\text{POCl}_3$ ). Finally, amination of **IV** using the relevant amine either in the presence of triethylamine in a microwave reactor or the palladium-catalyzed Buchwald–Hartwig aromatic amination reaction using a suitable ligand and base was employed to give the final compounds **V**: **1**, **3–7**, **10–15**, **21–30**, **32–38**, **40–53**, **57–61** and **2**, **8**, **9**, **16–20**, **31**, **39**, **54–56**, respectively. Hydrolysis of the chloro intermediate **IVa** using concentrated sulfuric acid produced the amide-containing intermediate **VIa**, which was subsequently aminated as in reaction iv to furnish the target compounds **58–60**. On the other hand, the use of the starting material **IIc**, containing a methyl ester group (**R**) instead of a nitrile, afforded the target compound **61**.

**Biology: Antiplasmodium Activity against Asexual Blood Stage Parasites.** With the aim of defining the SAR pattern around the PBI scaffold, synthesized analogues were first tested for their *in vitro* activity against the chloroquine-susceptible (CQS) *P. falciparum* NF54 strain.

**SAR1 Targets.** Structural modifications at SAR1 (Figure 1) produced compounds that may be classified broadly into either a *N*-linked ( $n = 0$ ; aniline-type) or *N*-methylene-linked ( $n = 1$ ; benzylamine-type) series (Figure 1). In the first series, the side group moiety comprises a phenyl ring directly linked to the PBI central core by a nitrogen. The electronic and lipophilic features of substitutions around the aromatic ring appeared to influence the antiplasmodium activity observed. For instance, unlike hydrophilic substituents, lipophilic groups on the aromatic side chains favored antiplasmodium activity. Active analogues in the low [**3** ( $\text{IC}_{50} = 1.16 \mu\text{M}$ ), **4** ( $\text{IC}_{50} = 1.01 \mu\text{M}$ ), **10** ( $\text{IC}_{50} = 0.17 \mu\text{M}$ ), and **13** ( $\text{IC}_{50} = 1.59 \mu\text{M}$ )] to moderate [**1** ( $\text{IC}_{50} = 2.14 \mu\text{M}$ ) and **5** ( $\text{IC}_{50} = 2.26 \mu\text{M}$ )] micromolar range were identified (Table 1). The most active derivative in the series was **10** ( $\text{IC}_{50} = 0.17 \mu\text{M}$ ), which had a

Scheme 1. General Scheme for Synthesis of the PBI Compounds<sup>a</sup>

<sup>a</sup>Reagents and conditions: (i) Ethyl cyanoacetate, DMF, 160 °C, 2 h, 61–76%; (ii) Ethyl 4,4,4-trifluoro-3-oxobutanoate, NH<sub>4</sub>OAc, 145 °C, 2 h, 27–66%; (iii) POCl<sub>3</sub>, (20 equiv), 130 °C, 3 h, 63–94%; (iv) Relevant amine (RNH<sub>2</sub>), Et<sub>3</sub>N, microwave, 80 °C, 150 W, 20–60 min (9–86%) or the appropriate amine, Pd<sub>2</sub>(dba)<sub>3</sub>, BINAP or Brettphos, K<sub>2</sub>CO<sub>3</sub> or Cs<sub>2</sub>CO<sub>3</sub>, toluene or 1,4-dioxane or *tert*-butanol, 100–120 °C, 12–16 h (6–54%); (v) concentrated sulfuric acid, 85 °C, 2 h, 89%. X, Y, Z, and R are as described in Tables 1–3.

trifluoromethoxy (–OCF<sub>3</sub>) substituent that combines both lipophilic and electron-withdrawing properties.

Introduction of a methylene linker ( $n = 1$ ; Figure 1) into the side group to extend the SAR from aniline-type to benzylamine-type series afforded analogues with antiplasmodium activities in the low micromolar range: **22** (IC<sub>50</sub> = 1.27 μM), **26** (IC<sub>50</sub> = 0.92 μM), and **34** (IC<sub>50</sub> = 1.49 μM) [Table 1]. As with the aniline-type series, lipophilic electron-withdrawing groups were equally favored in this series.

Isosteric replacement of the phenyl ring with various heteroaromatic groups produced diverse compounds including pyridyl (**17**, **30**, **31**, **32**), pyrimidyl (**16**, **19**, **39**), pyrazinyl (**29** and **20**), and thiazolyl (**18**) analogues (Table 1). Among them, only the pyridyl ring in the benzylamine series produced an active compound **30** (IC<sub>50</sub> = 1.16 μM). Interestingly, there seems to be a stringent requirement with regards to the positioning of the nitrogen on the pyridyl moiety, with only the 2 (ortho)-position (**30**; IC<sub>50</sub> = 1.16 μM) permitted for potency, while the 3 (*meta*)- and 4 (*para*)- positions produced compounds with lower activities, as observed for compounds **32** and **31**, respectively. On the other hand, replacement of the bulky aromatic side groups with the more polar, heterocyclic groups like piperazine was detrimental to activity, as seen with compound **40** (IC<sub>50</sub> = 10.03 μM) [Table 1].

The introduction of a methyl substituent on the nitrogen bridging the PBI core and the aromatic appendage (R, Figure 1) led to a decrease in activity, as illustrated by compound **23** (IC<sub>50</sub> > 2.72 μM), which bears a tertiary nitrogen, compared to its analogue **30** (IC<sub>50</sub> = 1.16 μM), in which this nitrogen is

secondary. This observation may suggest unfavorable steric interaction in the case of a tertiary nitrogen or the importance of hydrogen-bonding interactions, in the case of a secondary nitrogen, as in **30**, for suitable interactions with the target to take place, leading to the observed biological activity.

**SAR2 Analogues.** Target compounds in this subset were generated by modifications on the left-hand side (LHS) of the PBI core, as shown in Table 2. Following this modification, there was a general trend toward retention of, or improvement in, potency. For instance, **44** (IC<sub>50</sub> = 1.42 μM) is approximately equipotent to **30** (IC<sub>50</sub> = 1.16 μM; Table 1), while **43** (IC<sub>50</sub> = 0.44 μM) and **45** (IC<sub>50</sub> = 0.40 μM) are 2- to 4-fold as potent as their corresponding analogues lacking the dichloro modification, **26** (IC<sub>50</sub> = 0.84 μM; Table 1) and **34** (IC<sub>50</sub> = 1.49 μM; Table 1), respectively. Similarly, a nearly 5-fold improvement in potency was observed with **42** (IC<sub>50</sub> = 0.26 μM; Table 2), the dichloro substituted analogue of **22** (IC<sub>50</sub> = 1.28 μM; Table 1).

Further SAR iterations within this series revealed that the phenyl ring at SAR1 (R<sub>1</sub>, Figure 1) could be replaced with smaller heteroaromatic systems, such as furanyl **47** (IC<sub>50</sub> = 0.44 μM) and thiophene **48** (IC<sub>50</sub> = 0.31 μM) with retention of activity when accompanied by dichloro modifications at SAR2 (Y, Z = Cl, Table 2). However, replacement of the bulky aromatic side groups with more polar, heterocyclic groups like piperazine resulted in diminished activity, as seen with **51** (IC<sub>50</sub> = 8.11 μM). Poor antiplasmodium activity was observed among analogues in which the methylene linker ( $n = 1$ , SAR1, Figure 1) is substituted by the more polar sulfonyl group

**Table 1.** Antiplasmodium Potency of SAR1 Targets against Chloroquine-Susceptible (*PfNF54*) and Resistant (*PfK1*) Strains of *P. falciparum*

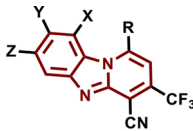
Compound Number	R	<sup>a</sup> Antiplasmodium activity IC <sub>50</sub> (μM)		Resistance Index	Compound Number	R	<sup>a</sup> Antiplasmodium activity IC <sub>50</sub> (μM)		Resistance Index
		<i>PfNF54</i>	<i>PfK1</i>				<i>PfNF54</i>	<i>PfK1</i>	
1		2.14			21		2.98		
2		2.36			22		1.27	0.89	0.7
3		1.16			23		>2.72		
4		1.01			24		6.11		
5		2.26			25		3.18		
6		5.62			26		0.92	0.84	0.91
7		>10			27		12.58		
8		>2.36			28		>2.68		
9		>2.32			29		2.60		
10		0.17	0.15	0.88	30		1.16	1.64	1.41
11		0.39	0.23	0.58	31		>2.72		
12		0.87	0.62	0.71	32		>2.72		
13		1.59			33		8.74		
14		>2.83			34		1.49		
15		>2.21			35		>2.36		
16		>2.82			36		>2.28		
17		>2.52			37		10.20		
18		>2.82			38		2.40		
19		>2.69			39		4.80		
20		4.42			40		10.03		

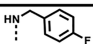
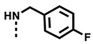
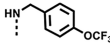
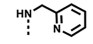
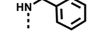
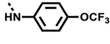
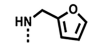
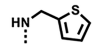
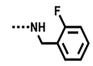
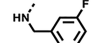
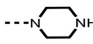
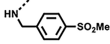
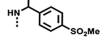
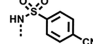
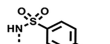
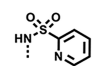
<sup>a</sup>Values are a mean of  $n \geq 2$  [<sup>3</sup>H]-hypoxanthine incorporation assays. IC<sub>50</sub> values generally differed less than 2-fold; those that varied above 3-fold were excluded from the analysis. <sup>b</sup>>IC<sub>50</sub> value is above the highest concentration used in the assay. Chloroquine and artesunate were used as controls whose established standard IC<sub>50</sub> values from  $n \geq 10$  determinations in our lab are 0.016 μM (*PfNF54*); 0.194 μM (*PfK1*) and 0.004 μM (*PfNF54*); 0.003 μM (*PfK1*), respectively.

(-SO<sub>2</sub>-), as observed with **55** (IC<sub>50</sub> = 6.73 μM) vs **43** (IC<sub>50</sub> = 0.44 μM), respectively (Table 2).

When comparing the position of the chloro groups on the LHS of the scaffold, the 3,5-dichloro analogue **41** (IC<sub>50</sub> = 0.21

μM) and the 4,5-dichloro compound **42** (IC<sub>50</sub> = 0.26 μM) were equipotent, indicating a negligible impact of regio-isomerism on this portion of the scaffold. On the contrary, regio-isomerism appears to be more important in the side

Table 2. Antiplasmodium Potency of SAR2 Targets against Chloroquine-Susceptible (*PfNF54*) and Resistant (*PfK1*) Strains of *P. falciparum*


Compound Number	X	Y	Z	R	<sup>a</sup> <i>In vitro</i> activity		Resistance Index
					IC <sub>50</sub> (μM)		
					<i>PfNF54</i>	<i>PfK1</i>	
41	Cl	H	Cl		0.31	0.21	0.68
42	H	Cl	Cl		0.44	0.28	0.64
43	H	Cl	Cl		0.44		
44	H	Cl	Cl		1.42		
45	H	Cl	Cl		0.40		
46	H	Cl	Cl		<sup>b</sup> >1.97		
47	H	Cl	Cl		0.44	0.23	0.52
48	H	Cl	Cl		0.31	0.14	0.45
49	H	Cl	Cl		0.17	0.14	0.82
50	H	Cl	Cl		0.19	0.15	0.79
51	H	Cl	Cl		8.11		
52	H	Cl	Cl		5.34	5.61	1.05
53	H	Cl	Cl		4.97		
54	H	Cl	Cl		5.64		
55	H	Cl	Cl		6.73	5.85	0.87
56	H	Cl	Cl		>6		

<sup>a</sup>Values are a mean of  $n \geq 2$  [<sup>3</sup>H]-hypoxanthine incorporation assays. IC<sub>50</sub> values generally differed less than 2-fold; those that varied above 3-fold were excluded from the analysis. <sup>b</sup>>IC<sub>50</sub> value is above the highest concentration used in the assay. Chloroquine and artesunate were used as

Table 2. continued

controls whose established standard  $IC_{50}$  values from  $n \geq 10$  determinations in our lab are  $0.016 \mu\text{M}$  (*Pf*NF54);  $0.194 \mu\text{M}$  (*Pf*K1) and  $0.004 \mu\text{M}$  (*Pf*NF54);  $0.003 \mu\text{M}$  (*Pf*K1), respectively.

Table 3. Antiplasmodium Potency of SAR3 Targets against Chloroquine-Susceptible (*Pf*NF54) and Resistant (*Pf*K1) Strains of *P. falciparum*

Compound Number	$R_1$	R	<sup>a</sup> <i>In vitro</i> activity		Resistance Index
			$IC_{50}$ ( $\mu\text{M}$ )		
			<i>Pf</i> NF54	<i>Pf</i> K1	
57	H		4.24	3.36	0.79
58	-CONH <sub>2</sub>		<sup>b</sup> >6		
59	-CONH <sub>2</sub>		5.16	7.59	1.47
60	-CONH <sub>2</sub>		>10	>10	
61	-COOMe		5.52		

<sup>a</sup>Values are a mean of  $n \geq 3$  determinations.  $IC_{50}$  values generally differed less than 2-fold; those that varied above 3-fold were excluded from the analysis. <sup>b</sup>> $IC_{50}$  value is above the highest concentration used in the assay. Chloroquine and artesunate were used as controls whose established standard  $IC_{50}$  values from  $n \geq 10$  determinations in our lab are  $0.016 \mu\text{M}$  (*Pf*NF54);  $0.194 \mu\text{M}$  (*Pf*K1) and  $0.004 \mu\text{M}$  (*Pf*NF54);  $0.003 \mu\text{M}$  (*Pf*K1), respectively.

groups at SARI. For example, moving the position of the substituents on the aromatic side group between the *ortho*, *meta*, and *para* positions resulted in **50** (*meta*,  $IC_{50} = 0.19 \mu\text{M}$ ) and **49** (*ortho*,  $IC_{50} = 0.17 \mu\text{M}$ ) being equipotent, and about twice as potent as analogue **42** (*para*,  $IC_{50} = 0.44 \mu\text{M}$ ) [Table 2].

**SAR3 Targets.** To explore effects on antiplasmodium activity by initiating structural changes around SAR3, analogues of previously active targets were prepared in which the nitrile at this position was replaced with other small groups, resulting in compounds **57** (H;  $IC_{50} = 4.24 \mu\text{M}$ ), **58** (CONH<sub>2</sub>;  $IC_{50} > 6 \mu\text{M}$ ), **59** (CONH<sub>2</sub>;  $IC_{50} = 5.16 \mu\text{M}$ ), **60** (CONH<sub>2</sub>;  $IC_{50} > 10 \mu\text{M}$ ), and **61** (COOMe;  $IC_{50} = 5.52 \mu\text{M}$ ) [Table 3]. The loss of antiplasmodium potency of these compounds compared with that of compounds **10**, **22**, **26**, and **30** suggests that a nitrile group at this site is required for activity.

Compounds with potent activity against the CQS *Pf*NF54 parasite strain ( $IC_{50} \approx 1 \mu\text{M}$ ) were also evaluated against the chloroquine-resistant (CQR) *Pf*K1 strain. Cross-resistance of these selected compounds with CQ was assessed by determining the fold change in the  $IC_{50}$  between the drug-sensitive and drug-resistant strains, expressed as the resistance index (RI), calculated as the ratio of  $IC_{50}$ *Pf*K1 to  $IC_{50}$ *Pf*NF54. Generally, activity trends were maintained across the two parasite strains (Tables 1–3). These results suggest that these

compounds are unlikely to demonstrate cross-resistance with CQ (RI = 12.1), as indicated by a less than 2-fold  $IC_{50}$  potency shift between the CQS and CQR parasite strains among the compounds.

**Inhibition of  $\beta$ -Hematin ( $\beta$ H) Formation.** Besides the ability to adopt a planar conformation, PBIs also have a rich electron density and protonatable nitrogen centers, features notably shared by aminoquinolines like CQ. This flat conformation, as demonstrated in CQ, is essential in facilitating  $\pi$ – $\pi$  interactions with heme molecules leading to inhibition of hemozoin (Hz) formation in *P. falciparum*.<sup>24</sup> The library of compounds generated in this study were evaluated for their ability to inhibit formation of  $\beta$ -hematin (synthetic Hz) in an *in vitro* setup designed to mimic the conditions of *P. falciparum* digestive vacuole (DV), the site of action of CQ.<sup>25</sup>

Most of the compounds displayed weak  $\beta$ -hematin inhibition ( $\beta$ HI) activity ( $IC_{50} > 100 \mu\text{M}$ ) (Table S1, Supporting Information). Only five compounds, **15** ( $IC_{50} = 50 \mu\text{M}$ ), **44** ( $IC_{50} = 59 \mu\text{M}$ ), **46** ( $IC_{50} = 32 \mu\text{M}$ ), **53** ( $IC_{50} = 32 \mu\text{M}$ ), and **55** ( $IC_{50} = 78 \mu\text{M}$ ) demonstrated  $\beta$ HI activity in the desired range ( $IC_{50} < 100 \mu\text{M}$ ), with **46** and **53** displaying the greatest potencies ( $IC_{50} = 32 \mu\text{M}$ ). In contrast, CQ, used as a positive control, displayed a  $\beta$ HI  $IC_{50}$  of  $18 \mu\text{M}$ .

The dichloro substitution on the LHS improved the  $\beta$ HI potency of **53** ( $IC_{50} = 32 \mu\text{M}$ ) compared to its analogue, **28**

( $IC_{50} > 100 \mu M$ ); a pattern also observed for **44** ( $IC_{50} = 59 \mu M$ ) vs **30** ( $IC_{50} > 100 \mu M$ ). A sulfonyl linker between the nitrogen attached to the PBI core and the aromatic portion of the side chain in the stead of a methylene group was detrimental to the potential to disrupt  $\beta H$  formation, as observed in the case of **56** ( $IC_{50} > 100 \mu M$ ) vs **44** ( $IC_{50} = 59 \mu M$ ). In addition, the chiral compound **53** ( $IC_{50} = 32 \mu M$ ) was more potent than its achiral analogue **52** ( $IC_{50} > 100 \mu M$ ), suggesting the role of the methyl substitution in offering additional beneficial interactions or facilitating suitable compound orientation for  $\beta HI$ .

There was no correlation between the antiplasmodium activity and the ability of this series to inhibit  $\beta H$  formation ( $R^2 = 0.04$ ,  $p$ -value = 0.19). Whereas the planar architecture of these compounds would be expected to impart  $\beta HI$  capabilities, as previously observed with analogous compounds,<sup>23,26</sup> it appears that the structural diversity pursued in this study introduced features that distorted the ability for appropriate binding to heme, leading to low  $\beta HI$  activities for most compounds. Nonetheless, owing to the presence of protonatable centers on these molecules, it is conceivable that intracellular DV accumulation might occur to sufficient concentrations that lead to inhibition of Hz formation. On the other hand, it is possible that these compounds elicit antiplasmodium activity via another mechanism independent from Hz inhibition. In fact, inhibition of  $\beta$ -1, 6-glucan synthase in fungi,<sup>27</sup> the lytic activity of pore-forming perforin,<sup>28</sup> and cytochrome *b* in trypanosomes<sup>29</sup> by other PBI derivatives has previously been reported.

**Plasmodium Life Cycle Activity Profiling of Front-runner Compounds.** To assess the ability of these compounds to potentially block malaria transmission as well as offer chemoprotection, the compounds displaying the highest potency against the parasite's asexual blood stages were evaluated for their activity against the liver stages of the rodent *P. berghei* parasite and against *P. falciparum* gametocyte stage. With reference to the liver stage activity profile, all tested compounds (Table 4) demonstrated *in vitro* submicromolar potency ( $IC_{50} = 0.06$ – $0.89 \mu M$ ) which was greater than that observed for primaquine ( $IC_{50} = 6.25 \mu M$ ), the control drug used in this assay. Among the compounds, **47**, **49**, and **50** demonstrated especially high activity with  $IC_{50}$  potencies of less than 100 nM. This is the first report of the liver stage activity of this series which indicates their prospects as antimalarial chemoprophylactic drug discovery leads. With tafenoquine having received US FDA approval only recently, primaquine is presently the only clinical compound widely used for radical cure of *P. vivax* and *P. ovale*-induced malaria.<sup>30</sup> However, despite the low *in vitro* activity observed with primaquine, the drug displays potent *in vivo* activity, which is attributed to its biotransformation to the active metabolite.<sup>31</sup> An accurate extrapolation of the *in vivo* potency of these compounds is therefore not possible based on direct comparisons with primaquine but will, rather, require animal experimentation in a model recapitulating the liver stage infection.

Based on the asexual blood stage activity observed for the compound library generated in this study, selected compounds were prioritized for the evaluation of their gametocytocidal potential. Ten analogues were subsequently tested against late stage gametocytes (>95% stage IV/V). Six compounds (**41**, **42**, **43**, **45**, **49**, and **50**) showed submicromolar  $IC_{50}$  values (Table 4) with **43** ( $IC_{50} = 0.21 \mu M$ ) the most potent, followed by **50**

**Table 4.** <sup>a</sup>Liver and Gametocyte Stage Activity of Selected Compounds

Compound Number	<i>Pb</i> Liver stage $IC_{50}$ ( $\mu M$ )	<i>Pf</i> NF54 Gametocyte activity	
		Final Late Stage $IC_{50}$ ( $\mu M$ )	$IC_{50}$ Fold Change (EG:LG/LG:EG) <sup>b</sup>
<b>10</b>	0.11	3.32	
<b>22</b>	0.89		
<b>26</b>	0.48		
<b>41</b>		0.74	3.0/0.3
<b>42</b>		0.69	
<b>43</b>	0.19	0.21	
<b>44</b>		2.48	
<b>45</b>		0.60	0.2/6.0
<b>47</b>	0.06	2.00	
<b>48</b>	0.14	1.67	
<b>49</b>	0.05	0.37	
<b>50</b>	0.07	0.27	1.2/0.5
Primaquine	6.25		
Methylene blue		0.9	
DHA		14	

<sup>a</sup>Values are the average of  $n \geq 3$  determinations.  $IC_{50}$  values generally differed less than 2-fold; those that varied above 3-fold were excluded from the analysis. <sup>b</sup>EG: Early stage gametocyte; LG: Late stage gametocyte. Final late stage  $IC_{50}$  represents the lowest of each value obtained for the luciferase reporter or ATP bioluminescence assay

( $IC_{50} = 0.27 \mu M$ ), **49** ( $IC_{50} = 0.37 \mu M$ ), **45** ( $IC_{50} = 0.60 \mu M$ ), **42** ( $IC_{50} = 0.69 \mu M$ ), and **41** ( $IC_{50} = 0.74 \mu M$ ). None of the compounds, except **45**, displayed increased activity toward the early stage gametocytes when compared to the late stages (Table 4). This is the first report of the gametocytocidal activity of this series, thereby reflecting the pan-active potential of the *N*-aryl-3-trifluoromethyl pyrido[1,2-*a*] benzimidazole scaffold.

Cumulatively, in view of the submicromolar potency of these compounds across the life cycle stages, these PBI derivatives are promising leads toward the identification of pan-active agents capable of preventing transmission and enabling chemoprevention. From the current antimalarial arsenal, over 90% of the drugs do not show potent activity toward late stage gametocytes and only primaquine and atovaquone have liver stage activities.<sup>23</sup>

**ADME and Cytotoxicity.** To select compounds for *in vivo* evaluation, compounds with the most potent *in vitro* asexual blood stage antiplasmodium activity were evaluated in terms of their cytotoxicity profile in the Chinese Hamster Ovarian cell line (Table 5). Generally, good selectivity indices (SI) were obtained in both the aniline-type and benzylamine-type series without manipulations on the LHS. In both subsets, all the compounds had an SI above 30 except for **34**, having a methyl substituent, that showed lower selectivity (SI = 17). Compounds **10**, **30**, and **26** displayed the best safety profiles (SI > 100). Interestingly, it appears that introducing a methylene bridge in the aromatic side chain of **10** (SI = 103) to give **26** (SI > 241) improves selectivity. Within the benzylamine series, better selectivity was achieved with **26** (SI > 241), which has the more lipophilic trifluoromethoxy substituent, compared to **22** (SI = 35) bearing a fluoro substituent. On the other hand, the methyl-substituted analogue **34** displayed the least attractive safety profile (SI = 17).

Table 5. *In Vitro* Metabolic Stability and Cytotoxicity Profiles of Frontrunner Analogues<sup>a</sup>

Compound Code	Structure	% rem. after 30min ( $t_{1/2min}$ )		<i>in vitro</i> IC <sub>50</sub> (μM)		Selectivity Index
		MLM	HLM	CHO	<i>Pf</i> NF54	
10		>99 (>150)	>99 (>150)	17.58	0.17	103
30		-	-	>272	1.16	>234
22		-	-	45	1.28	35
26		-	-	>222	0.92	>241
34		-	-	25	1.49	17
41		76 (75)	82 (105)	1.66	0.31	5
42		72 (63)	102 (>150)	13	0.44	30
43		82 (105)	>99 (>150)	5.02	0.44	11
44		31 (18)	72 (63)	0.75	1.42	0.5
45		69 (56)	91 (>150)	6.06	0.4	15
47		66 (50)	100 (>150)	4.84	0.44	10
48		-	-	8.48	0.31	27
49		84 (119)	97 (>150)	4.30	0.17	25
50		84 (119)	100 (>150)	7.03	0.19	37

<sup>a</sup>MLM: Mouse Liver Microsomes. HLM: Human Liver Microsomes. CHO: Chinese Hamster Ovarian Cell lines. %rem: Percent compound remaining after 30 min incubation.  $t_{1/2min}$ : Projected half-life in minutes. SI: selectivity index is the ratio of CHO IC<sub>50</sub>/*Pf*NF54IC<sub>50</sub>.

Table 6. hERG Inhibition Activity of Selected Compounds

Compound number	Chemical structure	% inhibition (SD) at	
		0.3 $\mu$ M	<sup>a</sup> IC <sub>50</sub> , $\mu$ M
10		7.51 (2.85)	>10
47		6.82 (2.81)	>10
48		6.13 (5.14)	>10
49		5.49 (3.90)	>10
50		6.53 (4.15)	>10

<sup>a</sup>Compounds showed less than 40% inhibition at the highest tested concentration of 10  $\mu$ M. All values represent the mean of three results obtained from experiments performed as biological and technical triplicates.

Notably, although the LHS modification whereby dichloro substitutions were performed improved the potency of many of the compounds, it also increased the potential for inducing cytotoxicity. Consequently, **22** (SI = 35), from which this modification is absent, displayed a better safety profile than both **41** (SI = 5) and **42** (SI = 30), which have reduced selectivity, whereas **34** (SI = 17) and **45** (SI = 15) have about the same selectivity profiles. Similarly, the excellent safety profile of **30** (SI > 234) was completely lost when dichloro groups were introduced at the LHS to give **44** (SI = 0.5).

Regio-isomerism of the LHS seems to impact the selectivity profiles of these compounds since **41** (SI = 5), with a 3,5 dichloro substitution pattern, is less selective than its 4, 5 dichloro-substituted analogue **42** (SI = 30). In contrast, regio-isomerism with respect to the position of substituents on the aromatic side group appears inconsequential to selectivity, as **42** (*para*-F, SI = 30), **49** (*ortho*-F, SI = 25), and **50** (*meta*-F, SI = 37) displayed similar selectivity indices. Overall, 2 out of the 14 compounds, **41** and **44**, failed to meet our defined criteria for compounds with good selectivity (SI > 10).

In general, the compounds showed moderate to high metabolic stability as assessed in mouse and human liver microsomes, MLM and HLM, respectively (Table 5). Compounds incorporating heteroaromatic moieties tended to be more labile, as exemplified by **44**, which had less than 75% of compound remaining after the 30 min incubation period in both HLM and MLM. Moreover, these compounds seem to be more efficiently metabolized in mouse than human microsomes, except for **10**, which was equally stable in both species. Overall, compounds with the highest microsomal stability in both species, with over 75% remaining after an incubation period of 30 min, were **10**, **49**, and **50**.

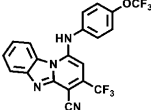
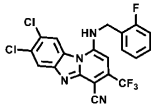
**hERG Inhibition Profiling.** Drugs that inhibit the hERG-encoded potassium ion channel can cause perturbations in myocardial function and lead to potentially fatal cardiac arrhythmias known as *torsade de pointes*.<sup>32,33</sup> For this reason, drug discovery programs often profile lead compounds against this target to establish any potential risk associated with the inhibition of this protein. To understand the potential for cardiotoxicity risk arising from possible off-target interactions with the hERG potassium ion channel, we profiled representative *in vitro* active compounds (**10**, **47**, **48**, **49**, and **50**) in the hERG assay using the IonWorks patch-clamp electrophysiology.<sup>34</sup> Experimental procedures for this assay are described in the Supporting Information (Section F) with data for the tested compounds summarized in Table 6.

This series showed a promising hERG potassium ion channel inhibition profile as depicted by the high IC<sub>50</sub> values (>10  $\mu$ M) [Table 6]. The positive control drug used in the experiment, verapamil hydrochloride, inhibited the target potently, with an IC<sub>50</sub> between 0.2 and 0.8  $\mu$ M.

**In Vivo Efficacy against the Blood Stage of *P. berghei* Infection.** Compounds **10** and **49**, representing leads from the aniline and benzylamine series, respectively, and possessing good *in vitro* ADME and cytotoxicity profiles, were selected for *in vivo* studies in a mouse model of malaria. NMRI mice infected intravenously with *P. berghei* parasites were treated 4 h, 24 h, 48 h, and 72 h postinfection with **10** and **49** at a dose of 50 mg/kg (4 × 50 mg/kg). Compound vehicle was administered to control mice. The *in vivo* efficacy was determined by comparing the parasitemia in the infected but untreated control mice and that of the treated animals. Animals were pronounced to have been cured if no parasitemia was detected 30 days after treatment.

Our results showed that treatment with **10** and **49** led to 98% and 99.9% reduction in blood parasitemia of the treated mice, respectively (Table 7). Furthermore, both treatments

**Table 7. Physicochemical Properties and Oral *in Vivo* Efficacy of 10 and 49 in NMRI Mice<sup>a</sup>**

	<b>10</b>	<b>49</b>
	 <p>Mw: 436.3 cLogP: 5.34 LogD: 5.34 TPSA: 62.35 Å<sup>2</sup> Sol: &lt;5 μM</p>	 <p>Mw: 453.2 cLogP: 5.73 LogD: 4.16 TPSA: 53.12 Å<sup>2</sup> Sol: &lt;5 μM</p>
Dose (mg/kg)	4x50	4x50
Reduction in parasitemia (%)	98	99.9
Mean survival days (MSD)	12	14

<sup>a</sup>Physicochemical data were computed using Chemdraw version 16.0 with solubility determined as described previously.<sup>23</sup>

increased animal survival relative to that of the control (MSD, 6 days), untreated group, with mean survival times of 12 and 14 days for **10** and **49**, respectively. In comparison, the reference drug used in the experiment, CQ, administered at a daily oral dose of 30 mg/kg for four consecutive days (4 × 30 mg/kg) achieved 99.9% reduction in parasitemia and resulted in a mean survival time of 21 days.

The modest improvements in the mice survival span achieved by **10** and **49** may possibly arise from inadequate pharmacokinetic properties that may limit bioavailability as has been reported previously for a related series of compounds<sup>22,23</sup> with solubility-limited absorption postulated to result in decreased systemic exposure. For poorly soluble compounds, the absorption is largely driven by lipophilicity. Consequently,

the absorption at a low dose may be comparable to that of a moderate dose since, at higher doses, the compound could precipitate in the gastrointestinal tract of the animal and is therefore not available for absorption. The presumed low exposure in the systemic circulation could result in suboptimal levels of the compound *in vivo*. Several factors relating to drug disposition including binding to proteins or tissues and clearance could modify *in vivo* outcomes. To investigate some of these possible scenarios, we performed pharmacokinetic (PK) analysis on one of the lead compounds, **10**, to understand the *in vivo* disposition of the series.

***In Vivo* Pharmacokinetics Analysis.** The PK profile of **10** was studied in mice, as a representative compound of the series. Oral disposition of the representative compounds **10** was studied in mice to enable investigation of the PK profile of this series. In this regard, C57B1/6 mice (*n* = 3) were dosed orally at 20 mg/kg while, in another set, the animals (*n* = 2 mice) were dosed intravenously at 2 mg/kg. Blood was sampled between 0 and 24 h at the intervals shown in Figure 2. Corresponding PK parameters were calculated using non-compartmental analysis and are presented in Table 8.

**Table 8. Oral and Intravenous Mouse Pharmacokinetics Parameters for 10**

Parameter	i.v. (2 mg/kg)	p.o. (20 mg/kg)
<i>C</i> <sub>max</sub> (μM)	—	1.1
<i>T</i> <sub>max</sub> (h)	—	5
<i>t</i> <sub>1/2</sub> (h)	11.4	7.86
<i>V</i> <sub>d</sub> (L/kg)	0.9	—
CL (mL/min/kg)	0.97	—
AUC <sub>0-∞</sub> (μM/L·min)	4774	1167
Oral bioavailability (%)	—	2

<sup>a</sup>For intravenous dosing (*n* = 2 mice), compounds were formulated in a solution of dimethylacetamide, polyethylene glycol and propylene glycol/ethanol mixture 4:1 at a ratio 1:3:6. <sup>b</sup>For oral dosing (*n* = 3 mice), compounds were formulated as suspension in 100% HPMC.

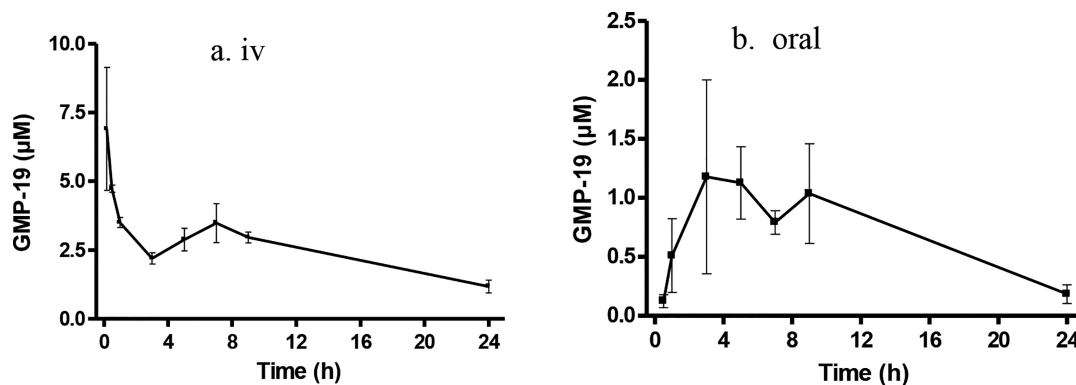


**Figure 2.** Pharmacokinetics profile for **10** following (a) intravenous (iv) and (b) oral administration. Each data point represents the mean from 2 (iv) and 3 (oral) mice with error bars indicating the standard deviation.

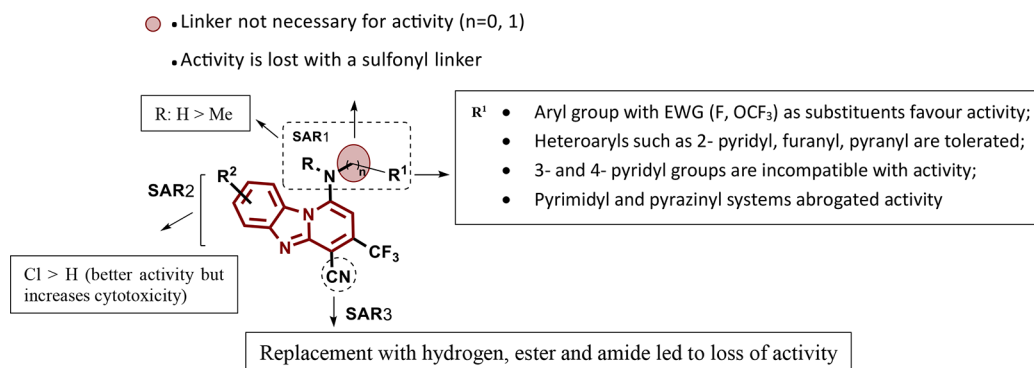


Figure 3. SAR trends summary.

Compound **10** displayed a delayed absorption profile ( $T_{\max}$  = 5 h) post-oral administration. At the oral dose of 20 mg/kg, the maximum concentration reached ( $C_{\max}$  = 1.1  $\mu\text{M}$ ) is 6-fold above the *in vitro*  $\text{IC}_{50}$  value (0.17  $\mu\text{M}$ ), and concentrations in blood remain above the *in vitro*  $\text{IC}_{50}$  for over 20 h. This is consistent with the good *in vivo* efficacy observed with these compounds [Table 8]. It should, however, be noted that the observed blood concentrations comprise both bound and free compound with the free fraction being credited with biological activity. Subsequent determination of the plasma protein binding profile for these compounds will be useful in establishing the actual free compound plasma concentration.

Taken together, the PK analysis of **10** suggests that this series displays delayed absorption, low volume of distribution, and low *in vivo* clearance. The meager bioavailability and variability in absorption, a frequent profile among compounds with poor solubility, highlights the need for optimizing this parameter toward improved PK and, potentially, oral efficacy. Further investigations are required toward understanding the tissue localization and distribution of these compounds. Based on the high *in vitro* metabolic stability, low *in vivo* clearance, and time above *in vitro*  $\text{IC}_{50}$  concentrations, these compounds are promising toward achieving long duration of antimalarial action. Ongoing studies are also aimed at understanding the resistance potential of this series through mutant generation.

## CONCLUSION

In conclusion, SAR studies were conducted around a PBI scaffold leading to the generation of *N*-aryl-3-trifluoromethyl pyrido[1,2-*a*]benzimidazoles with SAR trends as depicted in Figure 3. Compounds with not only submicromolar potency toward CQ-susceptible and multidrug resistant strains of *P. falciparum* but also maintained potency across multiple stages of the *Plasmodium* parasite's life cycle were identified.

Subsequent *in vitro* toxicity screening showed that the series has a favorable cytotoxicity profile including against the myocardial hERG-encoded potassium ion channel. Prioritized leads **10** and **49** elicited potent antimalarial efficacy leading to 98% and 99.9% reduction in parasitemia in mice accompanied by mean survival times of 12 and 14 days, respectively, when dosed orally at  $4 \times 50$  mg/kg. Pharmacokinetic analysis of **10** revealed that the series displays slow absorption, low volume of distribution, and low clearance profiles accompanied by low bioavailability. Further physicochemical optimization is ongoing to pursue these compounds as potential antimalarial leads with the potential not only to relieve clinical symptoms by targeting the asexual blood stages of *Plasmodium* but also to

offer chemoprotection and block transmission by killing liver and gametocytic forms of the parasite life cycle, respectively.

## EXPERIMENTAL SECTION

All commercially available chemicals were purchased from either Sigma-Aldrich or Combi-Blocks. All solvents were dried by appropriate techniques. Unless otherwise stated, all solvents used were anhydrous. <sup>1</sup>H NMR spectra were recorded at 300 or 400 MHz, and <sup>13</sup>C NMR spectra at 100 or 151 MHz, on a Bruker Spectrometer. Analytical thin-layer chromatography (TLC) was performed on aluminum-backed silica-gel 60 F<sub>254</sub> (70–230 mesh) plates. Column chromatography was performed with Merck silica-gel 60 (70–230 mesh). Chemical shifts ( $\delta$ ) are given in ppm downfield from TMS as the internal standard. Coupling constants, *J*, are recorded in hertz (Hz). Purity was determined by HPLC, and all compounds were confirmed to have >95% purity. The data that are not shown below are supplied in the Supporting Information (Section A).

**Preparation of 1-Hydroxy-3-(trifluoromethyl)benzo[4,5]-imidazo[1,2-*a*]pyridine-4-carbonitrile Intermediate IIIa.** Commercially sourced 2-(1H-benzo[*d*]imidazol-2-yl) acetonitrile **IIa** (1.0 equiv), ethyl 4,4,4-trifluoro-3-oxobutanoate (1.2 equiv), and ammonium acetate (2 equiv) were stirred at 145 °C for 2 h. The reaction mixture was cooled to 70 °C, and acetonitrile was added while stirring for a further 10 min. After cooling to room temperature, the mixture was filtered, residue was washed with acetonitrile, and the light-yellow product was obtained in 66% yield.

<sup>1</sup>H NMR (400 MHz, DMSO)  $\delta$  14.10 (bs, 1H), 8.60 (d, *J* = 8.2 Hz, 1H), 7.71–7.56 (m, 2H), 7.46 (ddd, *J* = 8.6, 6.8, 1.8 Hz, 1H), 6.43 (s, 1H); <sup>13</sup>C NMR (101 MHz, DMSO)  $\delta$  158.05, 148.14, 138.59, 132.21, 127.46, 123.92, 123.48, 121.36, 116.71, 114.62, 112.24, 103.27, 64.56.

LC-MS APCI+: found *m/z* = 278.1 [M + H]<sup>+</sup> (calcd for C<sub>13</sub>H<sub>6</sub>F<sub>3</sub>N<sub>3</sub>O: 277.0).

**Preparation of 1-Chloro-3-(trifluoromethyl)benzo[4,5]-imidazo[1,2-*a*]pyridine-4-carbonitrile Intermediate IVa.** Phosphoryl oxychloride (POCl<sub>3</sub>; 20 equiv) was added to 1-hydroxy-3-(trifluoromethyl)benzo[4,5]imidazo[1,2-*a*]pyridine-4-carbonitrile **IIIa** (1 equiv) and stirred at 130 °C for 3 h. Excess POCl<sub>3</sub> was removed under reduced pressure. On cooling to room temperature, ice cold water was added with consistent stirring for 15 min. The mixture was neutralized using sodium carbonate, and the crude product was filtered off, washed with water, dried at ambient conditions, and used subsequently without further purification. A resultant tan brown product was obtained in 91% yield.

<sup>1</sup>H NMR (300 MHz, DMSO)  $\delta$  8.74 (d, *J* = 8.6 Hz, 1H), 8.08 (d, *J* = 8.3 Hz, 1H), 7.81–7.71 (m, 2H), 7.65–7.56 (m, 1H); <sup>13</sup>C NMR (101 MHz, DMSO)  $\delta$  158.10, 147.99, 138.63, 132.31, 127.83, 123.93, 123.57, 121.09, 116.77, 114.60, 112.19, 103.32, 64.50.

LC-MS APCI+: found *m/z* = 296.0 (M + 1) (calcd for C<sub>13</sub>H<sub>5</sub>ClF<sub>3</sub>N<sub>3</sub>: 295.0).

**General Procedure for the Amination Step iv Using Microwave Irradiation: Method A.** The appropriate amine was added to a stirred mixture of the relevant chloro intermediate **IV** or

**VIa** (1.015 mmol, 1 equiv), triethylamine (2.03 mmol, 2 equiv), and tetrahydrofuran (THF) (4 mL) and subjected to microwave irradiation at 150 W, 80 °C for 20–40 min. The cooled reaction mixture was transferred to a round-bottom flask and concentrated. A minimum amount of either acetone or ethanol was added to precipitate the final product which was filtered off and dried. Occasionally, recrystallization in ethanol or column chromatography was performed to improve purity.

**General Procedure for the Amination Step iv Using Buchwald–Hartwig Conditions: Method B.** A mixture of the relevant chloro intermediate **IV**, the appropriate amine (1.2 equiv), Tris(dibenzylideneacetone) dipalladium(0), Pd<sub>2</sub>(dba)<sub>3</sub> (0.1 equiv), 2,2'-Bis(diphenylphosphino)-1,1'-binaphthyl (BINAP) (0.06 equiv) or BrettPhos (0.04 equiv) or RuPhos (0.1 equiv), potassium carbonate (K<sub>2</sub>CO<sub>3</sub>) or cesium carbonate (Cs<sub>2</sub>CO<sub>3</sub>) (3 equiv), and toluene/*tert*-butanol (1:1; 5 mL) or 1,4-dioxane (5 mL) were stirred in a sealed tube at 100–120 °C for 4–17 h. The cooled reaction mixture was stirred in ethyl acetate (50 mL) and water (100 mL) for 10–20 min. The separated organic layer was washed with water (2 × 50 mL), followed by saturated NaCl (2 × 50 mL), dried over magnesium sulfate, and filtered over Celite. The organic fraction was concentrated under reduced pressure, and ethanol was used to precipitate the crude product which was filtered to furnish the final product. In some cases, compounds were purified by recrystallization from ethanol or by column chromatography.

**Representative Final Compounds.** 1-((4-(Trifluoromethoxy)phenyl)amino)-3-(trifluoromethyl)benzo[4,5]imidazo[1,2-*a*]pyridine-4-carbonitrile **10**. Light green fluffy powder, 16% obtained from **IVa** using Method A.

<sup>1</sup>H NMR (400 MHz, DMSO) δ 8.82 (d, *J* = 8.1 Hz, 1H), 7.69 (d, *J* = 8.0 Hz, 1H), 7.64–7.54 (m, 1H), 7.46–7.42 (m, 1H), 7.39 (d, *J* = 8.3 Hz, 2H), 7.20 (d, *J* = 8.4 Hz, 2H), 6.24 (s, 1H). <sup>13</sup>C NMR (151 MHz, DMSO) δ 148.53, 144.88, 135.23, 133.74, 128.91, 127.21, 125.36, 123.71, 122.92, 122.71 (2C), 121.81, 121.58, 120.05, 119.68, 117.77 (2C), 115.20, 113.38, 95.93.

LC-MS APCI+: found *m/z* = 437.1 [M + H]<sup>+</sup> (calcd for C<sub>20</sub>H<sub>10</sub>F<sub>6</sub>N<sub>4</sub>O: 436.1).

1-((5,6-Dimethoxypyrimidin-4-yl)amino)-3-(trifluoromethyl)benzo[4,5]imidazo[1,2-*a*]pyridine-4-carbonitrile **16**. 17% from **IVa** using Method B.

<sup>1</sup>H NMR (300 MHz, DMSO) δ 9.08 (d, *J* = 10.1 Hz, 1H), 8.36 (s, 1H), 7.69 (d, *J* = 8.7 Hz, 1H), 7.67–7.59 (m, 1H), 7.52–7.43 (m, 1H), 7.40 (s, 1H), 4.00 (s, 3H), 3.80 (s, 3H). <sup>13</sup>C NMR (101 MHz, DMSO) δ 163.29, 162.70, 151.38, 147.54, 141.49, 135.42, 135.09, 128.73, 127.71 (2C), 124.15, 123.12 (2C), 121.42, 118.52, 114.91, 100.05, 60.64, 54.00.

LC-MS APCI+: found *m/z* = 415.1 [M + H]<sup>+</sup> (calcd for C<sub>19</sub>H<sub>13</sub>F<sub>3</sub>N<sub>6</sub>O<sub>2</sub>: 414.1).

1-(Pyrazin-2-ylamino)-3-(trifluoromethyl)benzo[4,5]imidazo[1,2-*a*]pyridine-4-carbonitrile **20**. 23% from **IVa** using Method B.

<sup>1</sup>H NMR (400 MHz, DMSO) δ 9.08 (d, *J* = 8.4 Hz, 1H), 8.54 (d, *J* = 1.4 Hz, 1H), 8.41 (dd, *J* = 2.7, 1.4 Hz, 1H), 8.25 (d, *J* = 2.7 Hz, 1H), 7.69 (ddd, *J* = 8.1, 1.2, 0.7 Hz, 1H), 7.63 (ddd, *J* = 8.2, 7.3, 1.1 Hz, 1H), 7.57 (s, 1H), 7.47 (ddd, *J* = 8.5, 7.3, 1.3 Hz, 1H). <sup>13</sup>C NMR (101 MHz, DMSO) δ 161.20, 156.43, 149.86, 147.99, 147.30, 142.50 (2C), 138.59, 135.58, 128.83, 127.54, 123.16, 118.91, 118.58, 114.80, 112.86, 99.37.

LC-MS APCI+: found *m/z* = 355.1 [M + H]<sup>+</sup> (calcd for C<sub>17</sub>H<sub>9</sub>F<sub>3</sub>N<sub>6</sub>: 354.1).

1-((4-(Trifluoromethoxy)benzyl)amino)-3-(trifluoromethyl)benzo[4,5]imidazo[1,2-*a*]pyridine-4-carbonitrile **26**. 49% from **IVa** via Method A.

<sup>1</sup>H NMR (300 MHz, DMSO) δ 8.71 (d, *J* = 8.4 Hz, 1H), 7.92 (d, *J* = 7.7 Hz, 1H), 7.72–7.60 (m, 3H), 7.49 (ddd, *J* = 8.4, 7.2, 1.2 Hz, 1H), 7.37 (dd, *J* = 8.8, 0.9 Hz, 2H), 6.31 (s, 1H), 4.95 (s, 2H). <sup>13</sup>C NMR (101 MHz, DMSO) δ 150.00, 148.48, 148.17, 137.28, 135.81, 133.84, 130.28, 129.51, 128.51, 127.00, 126.78, 124.13, 122.84, 121.48 (2C), 119.22, 115.75 (2C), 114.49, 86.73, 46.50.

LC-MS APCI+: found *m/z* = 451.1 [M + H]<sup>+</sup> (calcd for C<sub>21</sub>H<sub>12</sub>F<sub>6</sub>N<sub>4</sub>O: 450.1).

7,8-Dichloro-1-((4-fluorobenzyl)amino)-3-(trifluoromethyl)benzo[4,5]imidazo[1,2-*a*]pyridine-4-carbonitrile **42**. 22% from **IVc** according to Method A.

<sup>1</sup>H NMR (300 MHz, DMSO-*d*<sub>6</sub>) δ 9.03 (s, 1H), 7.69 (s, 1H), 7.52 (dd, *J* = 8.6, 5.6 Hz, 2H), 7.43 (dd, *J* = 8.4, 5.6 Hz, 2H), 6.00 (s, 1H), 4.59 (s, 2H). <sup>13</sup>C NMR (101 MHz, DMSO) δ 162.97, 160.18, 154.24, 150.99, 145.67, 139.02, 135.82, 134.57, 130.64, 129.58, 125.88, 119.90, 117.50, 116.55, 115.63, 115.57, 115.18, 100.00, 88.62, 43.67.

LC-MS APCI+: found *m/z* = 453.0 [M + H]<sup>+</sup> (calcd for C<sub>20</sub>H<sub>10</sub>Cl<sub>2</sub>F<sub>4</sub>N<sub>4</sub>: 452.0).

7,8-Dichloro-1-((2-fluorobenzyl)amino)-3-(trifluoromethyl)benzo[4,5]imidazo[1,2-*a*]pyridine-4-carbonitrile **49**. 58% from **IVc** via Method A.

<sup>1</sup>H NMR (300 MHz, DMSO-*d*<sub>6</sub>) δ 9.00 (s, 1H), 7.94 (s, 1H), 7.59 (t, *J* = 7.5 Hz, 1H), 7.40–7.12 (m, 3H), 6.22 (s, 1H), 4.79 (s, 2H). <sup>13</sup>C NMR (101 MHz, DMSO) δ 161.91, 159.49, 152.40, 150.75, 145.34, 136.58, 132.84, 131.42, 129.92, 129.22, 126.94, 127.87, 124.84, 121.78, 118.14, 117.37 (2C), 116.51, 115.46, 87.88.

LC-MS APCI+: found *m/z* = 453.0 [M + H]<sup>+</sup> (calcd for C<sub>20</sub>H<sub>10</sub>Cl<sub>2</sub>F<sub>4</sub>N<sub>4</sub>: 452.0).

**In Vitro Antiplasmodium Activity. Asexual Blood Stage Assay.** Compounds were screened against drug sensitive (NF54) and multidrug resistant (K1) strains of *P. falciparum* using the modified [<sup>3</sup>H]-hypoxanthine incorporation assay or the parasite lactate dehydrogenase assay (pLDH) as described in Supporting Information Section B.

**Gametocyte Activity.** *Pf*NF54 gametocytes were produced and late stage gametocytocidal IC<sub>50</sub> determinations were performed using the luciferase reporter and ATP bioluminescence platforms.<sup>22</sup> IC<sub>50</sub>'s were generated with Graphpad Prism 6, for *n* = 3 independent biological replicates performed in technical triplicates, ± SEM.

## ■ ASSOCIATED CONTENT

### Supporting Information

The Supporting Information is available free of charge on the ACS Publications website at DOI: 10.1021/acs.jmedchem.8b01769.

Additional details of the characterization of selected compounds and the procedures used for the *in vitro* and *in vivo* antimalarial and ADME studies as well as PK studies (PDF)

Molecular formula strings (CSV)

## ■ AUTHOR INFORMATION

### Corresponding Author

\*Phone: +27-21-6502553. Fax: +27-21-65045215. E-mail: Kelly.Chibale@uct.ac.za.

### ORCID

Timothy J. Egan: 0000-0001-7720-8473

Kelly Chibale: 0000-0002-1327-4727

### Notes

The authors declare no competing financial interest.

## ■ ACKNOWLEDGMENTS

The University of Cape Town (UCT), South African Medical Research Council, and South African Research Chairs Initiative of the Department of Science and Technology, administered through the South African National Research Foundation are gratefully acknowledged for support (K.C. and L.B. UID84627). At Swiss TPH, we thank Christoph Fischli, Sibylle Sax, Christian Scheurer and Ursula Lehmann for assistance in performing the antimalarial assays. At UCT, we thank Dr. Dale Taylor for running cytotoxicity assays and Trevor Finch for assistance with the animal work. At UP, we

thank Sindisiwe Nondaba for assistance in performing the gametocyte assays.

## ■ ABBREVIATIONS USED

ADME, absorption, distribution, metabolism and excretion; hERG, human ether-a-go-go-related gene; DMF, dimethylformamide; CHO cells, Chinese hamster ovarian cells; SAR, structure–activity relationships; CQ, chloroquine; MLM, mouse liver microsome; HLM, human liver microsomes; p.o., oral administration; i.v., intravenous administration; PK, pharmacokinetics; MSD, mean survival days; NMR, nuclear magnetic resonance; MS, mass spectrometry; POCl<sub>3</sub>, phosphoryl oxychloride; DMSO, dimethyl sulfoxide; Pd<sub>2</sub>(dba)<sub>3</sub>, Tris(dibenzylideneacetone) dipalladium(0); BINAP, 2,2′-Bis(diphenylphosphino)-1,1′-binaphthyl; SI, selectivity index

## ■ REFERENCES

- (1) World Health Organisation (WHO). *World Malaria Report*; Geneva, 2017.
- (2) Meshnick, S. R.; Dobson, M. J. The History of Anti-Malarial Drugs. *Antimalar. Chemother. Mech. Action, Resist. New Dir. Drug Discovery* **1948**, *14*, 14–16.
- (3) Freedman, D. O. Malaria Prevention in Short-Term Travelers. *N. Engl. J. Med.* **2008**, *359* (6), 603–612.
- (4) Garcia, C. R.; Markus, R. P.; Madeira, L. Tertian and Quartan Fevers: Temporal Regulation in Malarial Infection. *J. Biol. Rhythms* **2001**, *16* (321), 436–443.
- (5) Wells, T. N. C.; Burrows, J. N.; Baird, J. K. Targeting the Hypnozoite Reservoir of Plasmodium Vivax: The Hidden Obstacle to Malaria Elimination. *Trends Parasitol.* **2010**, *26* (3), 145–151.
- (6) Cox, F. E. History of the Discovery of the Malaria Parasites and Their Vectors. *Parasites Vectors* **2010**, *3*, 5.
- (7) Wells, T. N. C.; Alonso, P. L.; Gutteridge, W. E. New Medicines to Improve Control and Contribute to the Eradication of Malaria. *Nat. Rev. Drug Discovery* **2009**, *8* (11), 879–891.
- (8) Ridley, R. G. Medical Need, Scientific Opportunity and the Drive for Antimalarial Drugs. *Nature* **2002**, *415*, 686–693.
- (9) Olliaro, P. L.; Taylor, W. R. J. Antimalarial Compounds: From Bench to Bedside. *J. Exp. Biol.* **2003**, *206*, 3753–3759.
- (10) Flannery, E. L.; Chatterjee, A. K.; Winzeler, E. A. Antimalarial Drug Discovery — Approaches and Progress towards New Medicines. *Nat. Rev. Microbiol.* **2013**, *11* (12), 849–862.
- (11) Njoroge, M.; Njuguna, N. M.; Mutai, P.; Ongarora, D. S. B.; Smith, P. W.; Chibale, K. Recent Approaches to Chemical Discovery and Development Against Malaria and the Neglected Tropical Diseases Human African Trypanosomiasis and Schistosomiasis. *Chem. Rev.* **2014**, *114* (22), 11138–11163.
- (12) Sauerwein, R. W.; Roestenberg, M.; Moorthy, V. S. Experimental Human Challenge Infections Can Accelerate Clinical Malaria Vaccine Development. *Nat. Rev. Immunol.* **2011**, *11*, 57.
- (13) Crompton, P. D.; Pierce, S. K.; Miller, L. H. Advances and Challenges in Malaria Vaccine Development. *J. Clin. Invest.* **2010**, *120* (12), 4168–4178.
- (14) Amaratunga, C.; Sreng, S.; Suon, S.; Phelps, E. S.; Stepniewska, K.; Lim, P.; Zhou, C.; Mao, S.; Anderson, J. M.; Lindegardh, N.; Jiang, H.; Song, J.; Su, X.-Z.; White, N. J.; Dondorp, A. M.; Anderson, T. J. C.; Fay, M. P.; Mu, J.; Duong, S.; Fairhurst, R. M. Artemisinin-Resistant Plasmodium Falciparum in Pursat Province, Western Cambodia: A Parasite Clearance Rate Study. *Lancet Infect. Dis.* **2012**, *12* (11), 851–858.
- (15) Dondorp, A. M.; Fairhurst, R. M.; Slutsker, L.; MacArthur, J. R.; Breman, J. G.; Guerin, P. J.; Wellems, T. E.; Ringwald, P.; Newman, R. D.; Plowe, C. V. The Threat of Artemisinin-Resistant Malaria. *N. Engl. J. Med.* **2011**, *365* (12), 1073–1075.
- (16) Dondorp, A. M.; Nosten, F.; Yi, P.; Das, D.; Phyo, A. P.; Tarning, J.; Lwin, K. M.; Arie, F.; Hanpithakpong, W.; Lee, S. J.; Ringwald, P.; Silamut, K.; Imwong, M.; Chotivanich, K.; Lim, P.;

Herdman, T.; An, S. S.; Yeung, S.; Singhasivanon, P.; Day, N. P. J.; Lindegardh, N.; Socheat, D.; White, N. J. Artemisinin Resistance in Plasmodium Falciparum Malaria. *N. Engl. J. Med.* **2009**, *361* (5), 455–467.

(17) White, N. J.; Ashley, E. A.; Recht, J.; Delves, M. J.; Ruecker, A.; Smithuis, F. M.; Eziefula, A. C.; Bousema, T.; Drakeley, C.; Chotivanich, K.; Imwong, M.; Pukrittayakamee, S.; Prachumsri, J.; Chu, C.; Andolina, C.; Bancone, G.; Hien, T. T.; Mayxay, M.; Taylor, Walter R. J.; von Seidlein, L.; Price, R. N.; Barnes, K. I.; Djimde, A.; Kuile, F.; Gosling, R.; Chen, I.; Dhorda, M. J.; Stepniewska, K.; Guérin, P.; Woodrow, C. J.; Dondorp, A. M.; Day, N. P. J.; Nosten, F. H. Assessment of Therapeutic Responses to Gametocytocidal Drugs in Plasmodium Falciparum Malaria. *Malar. J.* **2014**, *13* (1), 483.

(18) Delves, M. J.; Angrisano, F.; Blagborough, A. M. Antimalarial Transmission-Blocking Interventions: Past, Present, and Future. *Trends Parasitol.* **2018**, *34* (9), 735–746.

(19) Sangani, C. B.; Jardosh, H. H.; Patel, M. P.; Patel, R. G. Microwave-Assisted Synthesis of Pyrido[1,2-a]Benzimidazole Derivatives of  $\beta$ -Aryloxyquinoline and Their Antimicrobial and Antituberculosis Activities. *Med. Chem. Res.* **2013**, *22* (6), 3035–3047.

(20) Takeshita, H.; Watanabe, J.; Kimura, Y.; Kawakami, K.; Takahashi, H.; Takemura, M.; Kitamura, A.; Someya, K.; Nakajima, R. Novel Pyridobenzimidazole Derivatives Exhibiting Antifungal Activity by the Inhibition of  $\beta$ -1,6-Glucan Synthesis. *Bioorg. Med. Chem. Lett.* **2010**, *20* (13), 3893–3896.

(21) Warriar, T.; Kapilashrami, K.; Argyrou, A.; Ioerger, T. R.; Little, D.; Murphy, K. C.; Nandakumar, M.; Park, S.; Gold, B.; Mi, J.; Zhang, Tuo.; Meiler, E.; Rees, Mike.; Somersan-Karakaya, S.; Porrás-De Francisco, E.; Martínez-Hoyos, M.; Burns-Huang, K.; Roberts, J.; Ling, Y.; Rhee, K. Y.; Mendoza-Losana, A.; Luo, M.; Nathan, Carl F. N-Methylation of a Bactericidal Compound as a Resistance Mechanism in Mycobacterium Tuberculosis. *Proc. Natl. Acad. Sci. U. S. A.* **2016**, *113* (31), E4523–E4530.

(22) Ndakala, A. J.; Gessner, R. K.; Gitari, P. W.; October, N.; White, K. L.; Hudson, A.; Fakorede, F.; Shackelford, D. M.; Kaiser, M.; Yeates, C.; Charman, S. A.; Chibale, K. Antimalarial Pyrido[1,2-a]Benzimidazoles. *J. Med. Chem.* **2011**, *54* (13), 4581–4589.

(23) Singh, K.; Okombo, J.; Brunshwig, C.; Ndubi, F.; Barnard, L.; Wilkinson, C.; Njogu, P. M.; Njoroge, M.; Laing, L.; Machado, M.; Prudêncio, M.; Reader, J.; Botha, M.; Nondaba, Sindisiwe; Birkholtz, L.-M.; Lauterbach, S.; Churchyard, A.; Coetzer, T. L.; Burrows, J. N.; Yeates, C.; Denti, P.; Wiesner, L.; Egan, T. J.; Wittlin, S.; Chibale, K. Antimalarial Pyrido[1,2-a]Benzimidazoles: Lead Optimization, Parasite Life Cycle Stage Profile, Mechanistic Evaluation, Killing Kinetics, and in Vivo Oral Efficacy in a Mouse Model. *J. Med. Chem.* **2017**, *60* (4), 1432–1448.

(24) Sullivan, D. J.; Gluzman, I. Y.; Russell, D. G.; Goldberg, D. E. On the Molecular Mechanism of Chloroquine's Antimalarial Action. *Proc. Natl. Acad. Sci. U. S. A.* **1996**, *93* (21), 11865–11870.

(25) Egan, T. J.; Hunter, R.; Kaschula, C. H.; Marques, H. M.; Misplon, A.; Walden, J. Structure–Function Relationships in Aminoquinolines: Effect of Amino and Chloro Groups on Quinoline–Hematin Complex Formation, Inhibition of  $\beta$ -Hematin Formation, and Antiplasmodial Activity. *J. Med. Chem.* **2000**, *43* (2), 283–291.

(26) Okombo, J.; Singh, K.; Mayoka, G.; Ndubi, F.; Barnard, L.; Njogu, P. M.; Njoroge, M.; Gibhard, L.; Brunshwig, C.; Vargas, M.; Keiser, J.; Egan, T. J.; Chibale, K. Antischistosomal Activity of Pyrido[1,2-a]Benzimidazole Derivatives and Correlation with Inhibition of  $\beta$ -Hematin Formation. *ACS Infect. Dis.* **2017**, *3* (6), 411–420.

(27) Kitamura, A.; Someya, K.; Hata, M.; Nakajima, R.; Takemura, M. Discovery of a Small-Molecule Inhibitor of  $\beta$ -1,6-Glucan Synthesis. *Antimicrob. Agents Chemother.* **2009**, *53* (2), 670–677.

(28) Lyons, D. M.; Huttunen, K. M.; Browne, K. A.; Ciccone, A.; Trapani, J. A.; Denny, W. A.; Spicer, J. A. Inhibition of the Cellular Function of Perforin by 1-Amino-2,4-Dicyanopyrido[1,2-a]-Benzimidazoles. *Bioorg. Med. Chem.* **2011**, *19* (13), 4091–4100.

(29) Khare, S.; Roach, S. L.; Barnes, S. W.; Hoepfner, D.; Walker, J. R.; Chatterjee, A. K.; Neitz, R. J.; Arkin, M. R.; McNamara, C. W.; Ballard, J.; Lai, Yin.; Fu, Y.; Molteni, V.; Yeh, V.; McKerrow, J. H.; Glynn, R. J.; Supek, Frantisek. Utilizing Chemical Genomics to Identify Cytochrome b as a Novel Drug Target for Chagas Disease. *PLoS Pathog.* **2015**, *11* (7), No. e1005058.

(30) John, G. K.; Douglas, N. M.; von Seidlein, L.; Nosten, F.; Baird, K. J.; White, N. J.; Price, R. N. Primaquine Radical Cure of *Plasmodium Vivax*: A Critical Review of the Literature. *Malar. J.* **2012**, *11* (1), 280.

(31) Pybus, B. S.; Marcsisin, S. R.; Jin, X.; Deye, G.; Sousa, J. C.; Li, Q.; Caridha, D.; Zeng, Q.; Reichard, G. A.; Ockenhouse, C.; Bennett, J.; Walker, L. A.; Ohrt, C.; Melendez, V. The Metabolism of Primaquine to Its Active Metabolite Is Dependent on CYP 2D6. *Malar. J.* **2013**, *12* (1), 212.

(32) Raschi, E.; Ceccarini, L.; De Ponti, F.; Recanatini, M. HERG-Related Drug Toxicity and Models for Predicting HERG Liability and QT Prolongation. *Expert Opin. Drug Metab. Toxicol.* **2009**, *5* (9), 1005–1021.

(33) Braga, R.; Alves, V.; Silva, M.; Muratov, E.; Fourches, D.; Tropsha, A.; Andrade, C. Tuning HERG Out: Antitarget QSAR Models for Drug Development. *Curr. Top. Med. Chem.* **2014**, *14* (11), 1399–1415.

(34) Bridgland-Taylor, M. H.; Hargreaves, A. C.; Easter, A.; Orme, A.; Henthorn, D. C.; Ding, M.; Davis, A. M.; Small, B. G.; Heapy, C. G.; Abi-Gerges, N.; Persson, F.; Jacobson, L.; Sullivan, M.; Albertson, N.; Hammond, T. G.; Sullivan, E.; Valentin, J.-P.; Pollard, C. E. Optimisation and Validation of a Medium-Throughput Electrophysiology-Based HERG Assay Using IonWorks<sup>TM</sup> HT. *J. Pharmacol. Toxicol. Methods* **2006**, *54* (2), 189–199.